JTTEE5 21:1076–1082
DOI: 10.1007/s11666-012-9787-5
1059-9630/$19.00 © ASM International

Evaluation of Microstructural Evolution of Nanostructured Yttria-stabilized Zirconia During Sintering Using Impedance Spectroscopy

Chenchen Ge, Liyong Ni, and Chungen Zhou

(Submitted February 13, 2012; in revised form March 25, 2012)

A non-destructive evaluation (NDE) technique of impedance spectroscopy (IS) was employed for studying the sintering process of nanostructured yttria-stabilized zirconia (YSZ) after exposure at 1100 °C in air for different times. The variations within microstructure of YSZ were correlated with the EIS parameters. The results showed that the resistance and capacitance of YSZ grains (g) and grain boundaries (gb) varied with the sintering time. The resistance of YSZ g and gb increased significantly in 10 h, which may correspond to closure of pores. While during the stage from 10 to 200 h, the resistance of the g was basically consistent, and the gb decreased with the growth of g, which indicated that the gb resistance was more sensitive to grain size. The change of porosity and pore shape could be interpreted through impedance parameters. The porosity decreased and the shape of pores became smaller and rounder with the increasing sintering time.

Keywords grain growth, impedance spectroscopy, nanostructured thermal barrier coating, pores

1. Introduction

Thermal barrier coatings (TBCs) have been widely used in the hot sections of gas turbines as they provide the potential to raise efficiency and operating time of the devices (Ref 1, 2). A typical duplex TBC system is composed of a heat-insulating ceramic top coating and an oxidation-resistant metallic bond coating. ZrO_2 partially stabilized Y_2O_3—yttria-stabilized zirconia (YSZ)—is commonly used as ceramic top coat because of its low thermal conductivity and high coefficient of thermal expansion. The YSZ is generally deposited by air plasma spraying (APS), or electron beam physical vapor deposition (Ref 3).

Nanostructured YSZ coatings have recently drawn much attention because of their outstanding properties. It has been confirmed (Ref 4-7) that nanostructured YSZ coatings have lower thermal conductivity, higher coefficient of thermal expansion, and more excellent mechanical properties compared with traditional YSZ coatings. However, the grain growth and the closure of pores would occur during sintering, consequently leading to the disappearance of the nanostructure and superior properties. Thus, it is important to develop a non-destructive evaluation (NDE) method to monitor the microstructural evolution of the nano-TBCs during thermal exposure.

At present, impedance spectroscopy (IS) has been used to study the degradation of ceramic materials owing to its simplicity and accuracy (Ref 8-14). Also, impedance measurements can measure the microstructural evolution of TBCs without the restriction of sizes of samples and noises from environment, compared with other NDE techniques, such as photoluminescence for showing the residual stress and phase content of thermally grown oxide (TGO) layer (Ref 15, 16), and acoustic emission for the examination of cracks in TBCs (Ref 17, 18). Since Ogawa et al. (Ref 8) applied IS as a NDE tool to studying the degradation of APS TBCs, a great many studies have been focused on the NDE of TBCs by means of IS. Xiao and co-workers (Ref 9-11) and Sohn et al. (Ref 12-14) utilized impedance measurement methods to study the microstructural evolution of conventional TBC system, such as TGO growth, phase transformations and porosity of YSZ topcoat, and cracks at the TGO/BC interface.

Because the nanostructured YSZ is a porous material, the electrical properties of microstructure were affected significantly by porosity (Ref 19-21). In the present study, the aim is to evaluate microstructural evolution of nanostructured TBCs at 1100 °C for different thermal exposure times using IS along with scanning electron microscopy (SEM) and x-ray diffractometer (XRD). The correlation of microstructure of TBC with its electrical properties after thermal exposure has been investigated.

Chenchen Ge, Liyong Ni, and **Chungen Zhou**, Department of Materials Science and Engineering, Beijing University of Aeronautics and Astronautics, Key Laboratory of Aerospace Materials and Performance (Ministry of Education), Beijing 100191, China. Contact e-mail: cgzhou@buaa.edu.cn.

2. Experimental Procedures

2.1 Sample Preparation

The 7-8 wt.% Y_2O_3 partially stabilized the nanostructured zirconia powder with the grain size of 15-35 nm, was sprayed by APS on the stainless steel substrate. The powder was agglomerated into 50-80 μm particles before the APS was applied. The parameters of plasma spraying have been reported in our previous study (Ref 22, 23). The specimens used for sintering were put into cold water immediately after spraying. The coating was detached from the stainless steel, then polished into 1.5 mm in thickness. The heat-treatment experiments of the free-standing coatings were performed at 1100 °C for 10 h, 50, 100, and 200 h, respectively.

2.2 Impedance Measurement

Each of the YSZ sides was coated with a platinum paint with an area of 5 × 5 mm^2, which served as one of the electrodes. For consolidating the platinum paints and enhancing their adhesion to the specimen surfaces, the paints were baked at 800 °C for 15 min. Impedance measurements were performed at 400 °C using a Solartron SI 1255 HF frequency response analyzer connected with a computer-controlled Solartron 1296 Dielectric Interfaces. The measurements were carried out with AC amplitude of 100 mV and AC frequency of 1-10^7 Hz. Spectra analysis (fitting) was made by means of Zview impedance analysis software (Scribner Associates Inc., Southern Pines, NC) to obtain the electrical properties of YSZ.

2.3 Microstructural Examination

The evolution of microstructure of nanostructured YSZ was analyzed using S-3500 scanning electron microscope (Hitachi, Tokyo, Japan). The phase identification was carried out using a D/max 2200pc x-ray diffractometer (Cu K_α radiation; Rigaku, Tokyo, Japan).

3. Results and Discussion

3.1 Microsructure of the Coatings

Figure 1 shows the typical fractured cross section of the as-sprayed nanostructured YSZ coating. It is seen from Fig. 1 that there are two kinds of regions in the coating: the molten phase and the non-molten phase. The structure of the non-molten phases is very loose, containing the equiaxed grains and nanosized grains, and the macropores between nano-particles have sizes similar to these particles. This structure will enhance thermal insulation ability of TBC coating.

The XRD patterns of YSZ exposed to air at 1100 °C for different times are presented in Fig. 2. The coatings before and after sintering consist of tetragonal phase zirconia indicate that there are no new phases being generated within the coating during sintering.

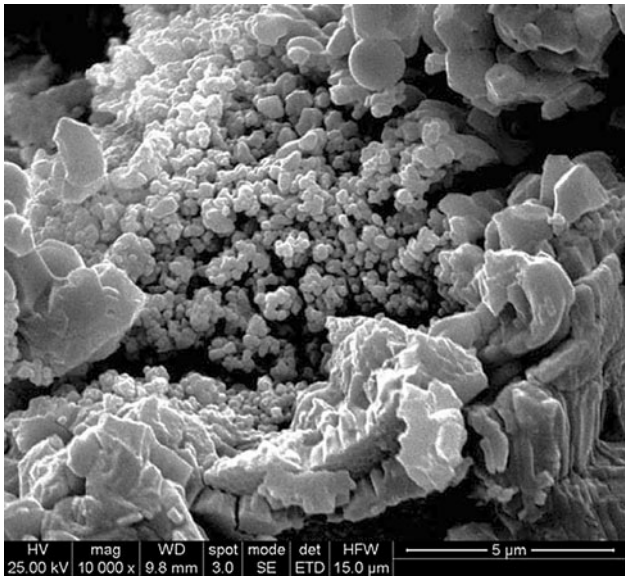

Fig. 1 The microstructure of the as-sprayed nanostructured YSZ coatings

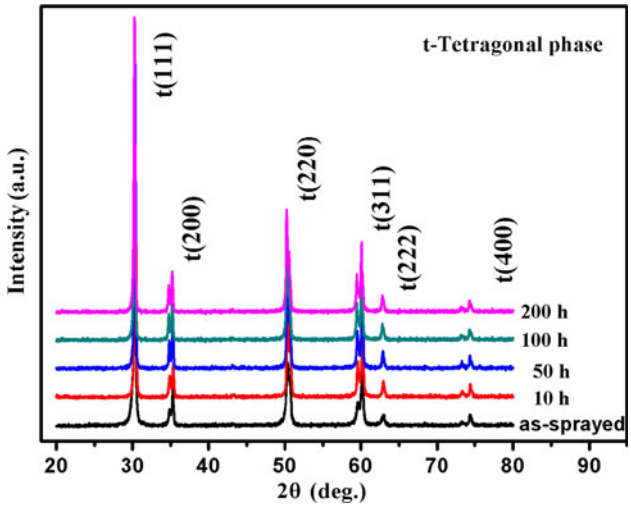

Fig. 2 The XRD patterns of YSZ before and after thermal exposure for different times at 1100 °C

3.2 Impedance Spectra and Equivalent Circuit Modeling

Figure 3(a) shows typical Bode plots [phase angle (θ) vs. log frequency] after thermal exposure for 0, 10, 50, 100, and 200 h. The graphs show a number of electrical responses. There are three relaxation processes for the specimens. For all the specimens, the three relaxation processes shown in the spectra are separately attributed to YSZ grains (g) (approximately 10^6 Hz), YSZ grain boundaries (gb) (approximately 10^4 Hz), and the electrode response (E) (approximately 1 Hz). The difference in the intrinsic electrical properties of g and gb lead to the distinction of responses in the impedance spectra. These

phenomena have been confirmed in previous studies concerning heat treatment on YSZ and high temperature oxidation of the TBCs (Ref 14, 24). Nyquist plots [imaginary impedance (Z'') vs. real impedance (Z')] of the specimens exposed to air for different times are shown in Fig. 3(b). Two semicircles are presented in Nyquist plot, corresponding to YSZ grain and YSZ grain boundary, and the big tail is attributed to the electrode reaction. For the short sintering time, two poorly resolved semicircles are observed, and the separation of the two semicircles is obvious with the increasing sintering time.

To set up a linkage with the evolution of the microstructure of YSZ, impedance plots should be simulated by establishing an equivalent circuit model. In general, an equivalent circuit model could contain several units in series, and each unit consists of one resistor and one capacitor in parallel. Because the measured capacitance response is often not ideal (Ref 25, 26), constant phase element (CPE) could be used instead of an ideal capacitance element in the equivalent circuit. The impedance of CPE is given by Ref 25

$$Z_{\mathrm{CPE}} = A^{-1}(jw)^{-n} \quad \text{(Eq 1)}$$

where A is a parameter that is independent of frequency, and n is an exponential index that characterizes a dispersion of relaxation frequency. When $n=0$, CPE acts as a pure resistor; when $n=1$, the CPE represents an ideal capacitor. Thus, CPE can correspond to a wide range of non-ideal capacitance elements that could be more suitable to describe the electrical properties of TBCs. Here, the capacitance can be calculated according to Ref 27

$$C = R^{(1-n)/n}A^{1/n} \quad \text{(Eq 2)}$$

where R is the resistance.

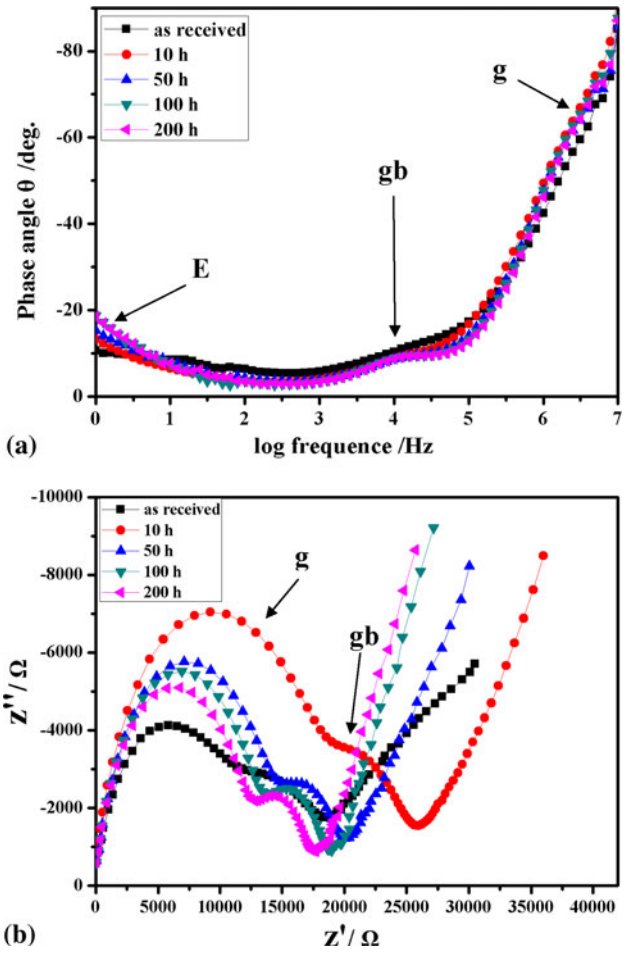

Fig. 3 Impedance spectra measured after YSZ exposed at 1100 °C for different times (a) Bode plots and (b) Nyquist plots

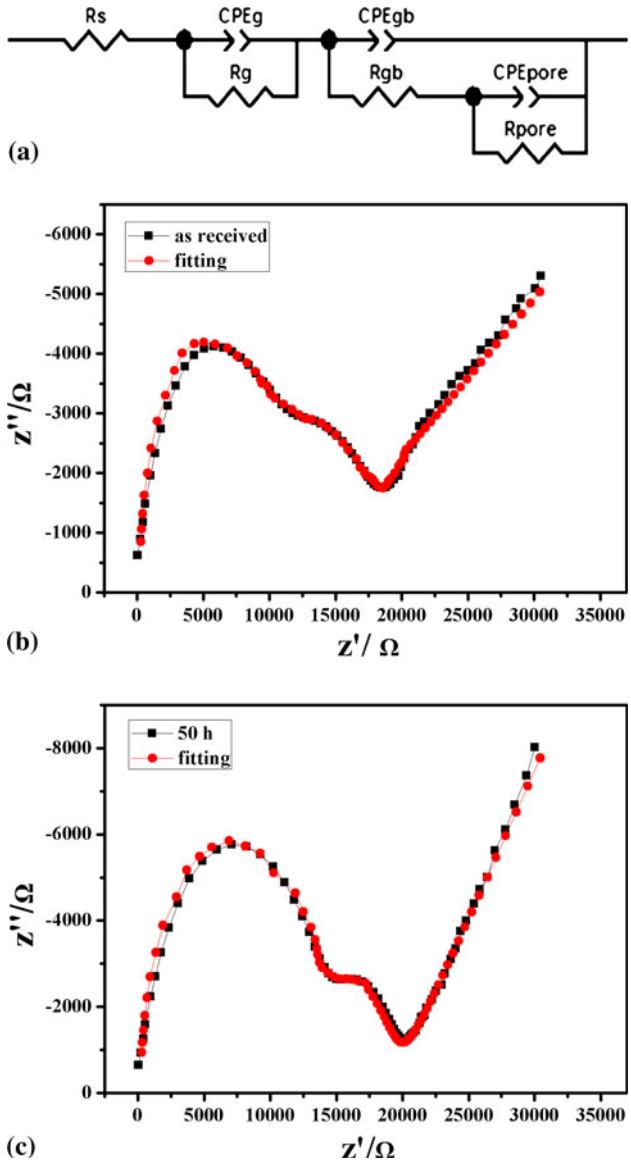

Fig. 4 (a) Equivalent circuit models for nanostructured YSZ before and after thermal exposure; measured impedance spectra and fitted results of YSZ (b) as received; (c) after exposed to air at 1100°C for 50 h

The traditional brick-layer model is commonly employed to analyze the electrical behavior of dense ceramic materials. However, its application in the case of highly porous ceramics such as nanostructured YSZ is inappropriate. An ac equivalent circuit for the porous YSZ is constructed as shown in Fig. 4(a) where R_g and CPE_g correspond to YSZ grain, R_{gb} and CPE_{gb} correspond to YSZ grain boundary, and R_{pore} and CPE_{pore} correspond to the pores in YSZ. Actually, a contribution from the porosity to the impedance plot has been proposed (Ref 28) using IS. The contribution is composed of a small semicircle positioned between the high-frequency grain semicircle and the lower-frequency grain boundary semicircle. The relaxation frequency of the high porosity was close to gb and could not contribute separately to the impedance plot. Hence, two responses are being seen in impedance plots. Based on the model, Nyquist plot can be simulated very well (Fig. 4b, c), and the values of *R*, A, and n of all the equivalent elements can be obtained from the software. The C values can be calculated by Eq 2. According to the equivalent circuit model established above, spectra analysis was performed using Zview impedance analysis software to fit the electrical parameters of YSZ.

3.3 Electrical Properties and Their Relation to Microstructural Features

Figure 5 shows the morphology of the non-molten particles after thermal exposure for different times at 1100 °C. The size of the g increases with the increasing sintering time and the YSZ coating has lost its nanostructure after 50 h. The micrographs of the cross section of the polished TBCs for the as-sprayed at 10-, 50-, and 100-h exposures are presented in Fig. 6. It is obvious that the size and number of pores decreased rapidly during the sintering stage of the first 10 h (densification regime), then slowly during the 10-200-h exposure (grain-growth regime). A trend showing that the shape of pores existing in TBCs is rounder and smaller during sintering is observed.

The impedance response detected by the system depends on the microstructural features of the materials such as g, gb, and pores. Variations in the electrochemical resistance and capacitance of the grain and grain boundary,

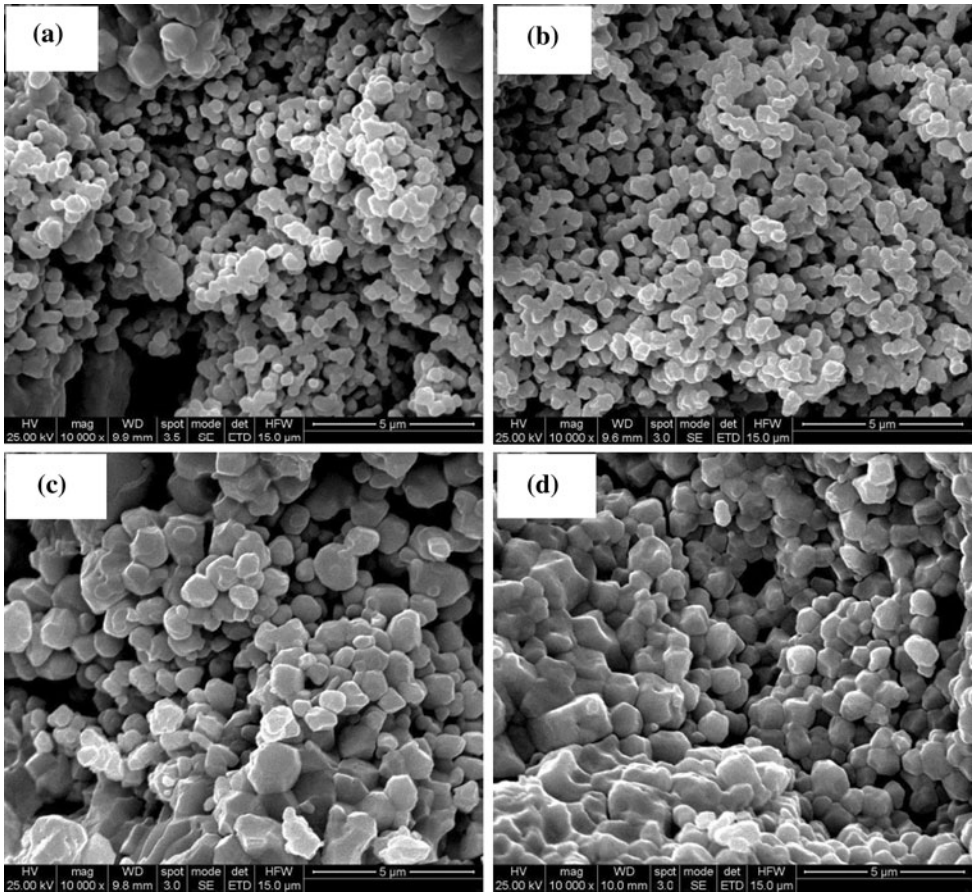

Fig. 5 SEM of the fractured cross sections of nano-YSZ coatings before (a) and after sintering at 1100 °C for (b) 10 h; (c) 50 h; and (d) 100 h

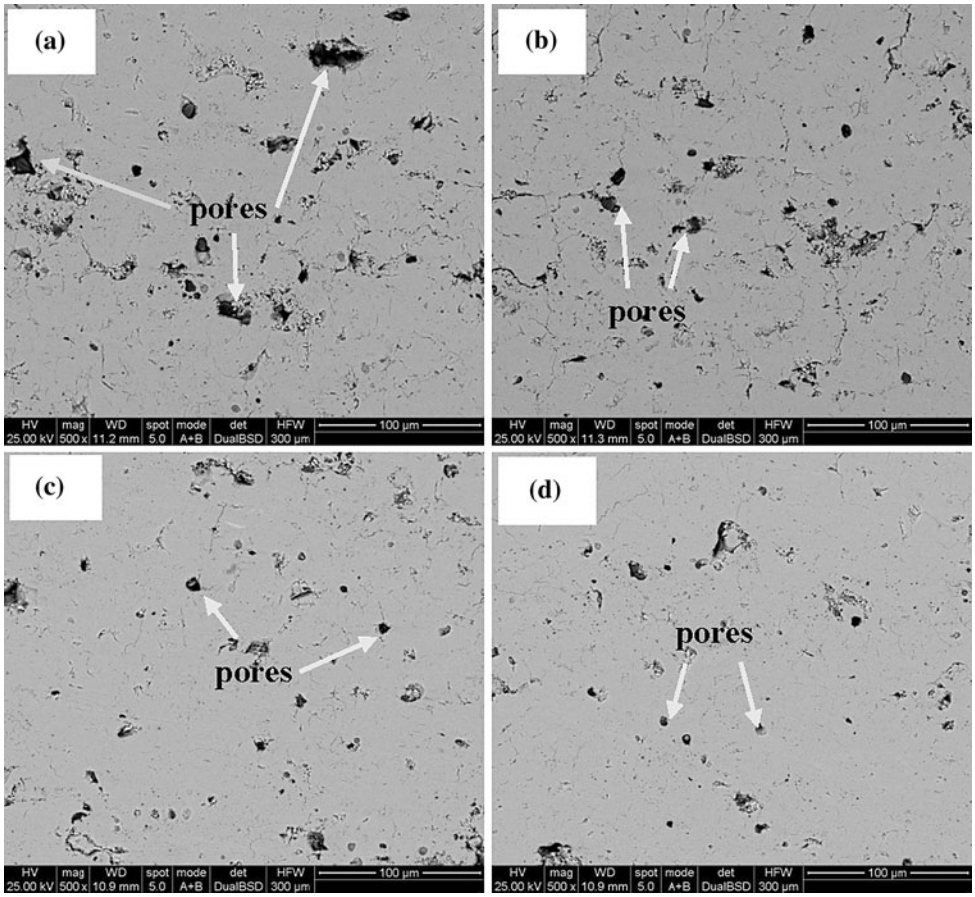

Fig. 6 The polished cross sections of nanostructured TBCs before (a) and after sintering at 1100 °C for (b) 10 h; (c) 50 h; (d) 100 h

namely, R_g, C_g, R_{gb}, and C_{gb}, as a function of thermal exposure at 1100 °C are shown in Fig. 7. By XRD, no evidence of phase transformations was observed, and so it appears that the variations are microstructurally controlled. An abrupt increase in the R_g is observed during the first 10 h, and then no significant change is observed during the sintering from 10 to 200 h (Fig. 7a). Since the conductivity of grain is dependent on density and is insensitive to grain size (Ref 29-31), the increase of the resistance of YSZ grain initially is caused by pores' closure, and then there is no significant change when g grow. The pores can be considered as a number of capacitances in a parallel circuit, in which the capacitance of all the pores equals to the sum of capacitance of each pore. Therefore, the capacitance of YSZ grain decreases with pores closure and then increases a little higher until reaching a stable condition because of g growing and closing of a few pores. Similar to R_g, the increase of R_{gb} up to 10 h is observed with the increased thickness of grain boundary owing to pores closure (Fig. 7b). The decrease in R_{gb} is caused by a decrease in the volume fraction of gb with g growing during thermal exposure from 10 to 200 h. The capacitance of YSZ grain boundary changes slowly in the densification regime and has an abrupt increase for the grain-growth regime, which indicate that the change of C_{gb} is attribute to grain size occurring on the relative density.

The CPE parameters of pores, A_{pore} and n_{pore} as function of the sintering time are shown in Fig. 8. As mentioned, CPE is used instead of capacitance because of the capacitor not being ideal. The more homogenous and uniform the structure is, the closer the value of index n is to 1. For the pores existing in YSZ layer, the parameter A_{pore} shows a decreasing trend with sintering time, because of the closure of pores in the YSZ layer during sintering. The index n_{pore} shows an increasing trend, which indicates that the homogeneity of pores increases during the sintering process. These results are in accordance with the phenomena shown in Fig. 6.

4. Conclusions

In this study, the microstructural evolution of a plasma-sprayed nanostructured TBC exposed in air at 1100 °C was investigated by means of IS in conjunction with SEM and XRD. The major results are as follows:

For the YSZ grain, R_g increased and C_g decreased within 10 h, because of the closure of pores in YSZ layer.

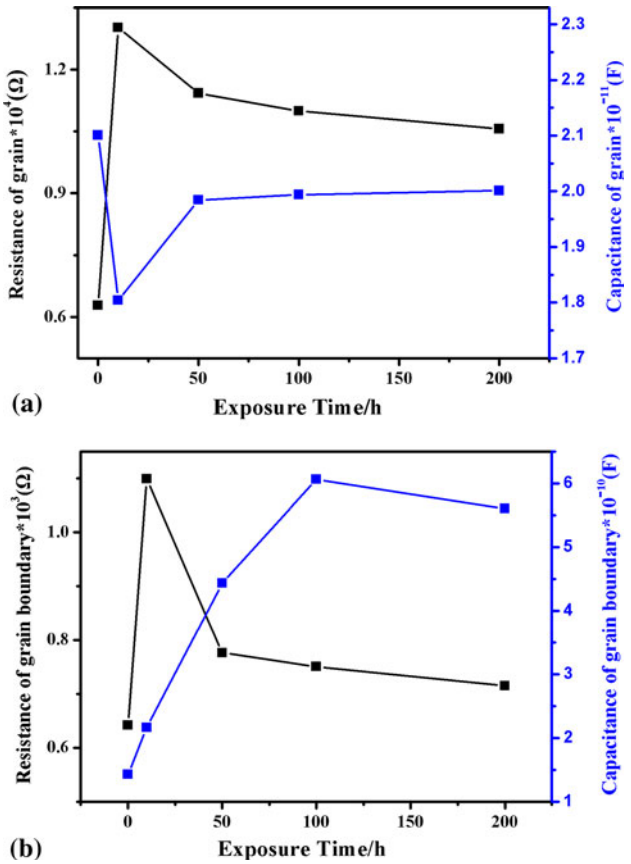

Fig. 7 Variations in resistance and capacitance of (a) YSZ grain and (b) YSZ grain boundary as a function of exposure time after sintering at 1100 °C

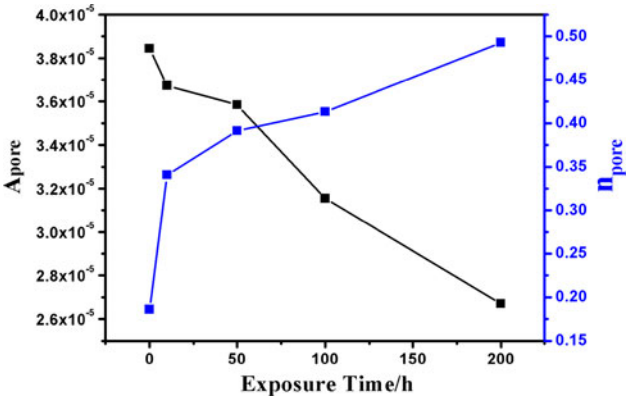

Fig. 8 CPE parameters of nano-YSZ as a function of exposure time after sintering at 1100 °C

The effect of grain growth on R_g and C_g could be neglected for the duration from 10 to 200 h. For the YSZ grain boundary, R_{gb} increased within 10 h because of pore closure and then decreased during 10-200 h when grain growth occurred. The C_{gb} increased with sintering time, which may be linked to the level of grain size. The decreased A_{pore} indicated the reduction of porosity, and the increased n_{pore} revealed that the shape of pores became more uniform with sintering time.

Acknowledgments

This work was supported by the Aviation Science Foundation of 2011ZF51062.

References

1. N.P. Padture, M. Gell, and E.H. Jordan, Thermal Barrier Coatings for Gas Turbine Engine Applications, *Science*, 2002, **296**, p 280-284
2. A.G. Evans, M.Y. He, and J.W. Hutchinson, Mechanics-Based Scaling Laws for the Durability of Thermal Barrier Coatings, *Prog. Mater. Sci.*, 2001, **46**(3-4), p 249-271
3. U. Schulz, K. Fritscher, and M. Peters, EB-PVD Y_2O_3-and CeO_2/Y_2O_3-Stabilized Zirconia Thermal Barrier Coatings—Crystal Habit and Phase Composition, *Surf. Coat. Technol.*, 1996, **82**, p 259-269
4. C.G. Zhou, N. Wang, Z.B. Wang, S.K. Gong, and H.B. Xu, Thermal Cycling Life and Thermal Diffusivity of a Plasma-Sprayed Nanostructured Thermal Barrier Coating, *Scr. Mater.*, 2004, **51**(10), p 945-948
5. R.S. Lima and B.R. Marple, Nanostructured YSZ Thermal Barrier Coatings Engineered to Counteract Sintering Effects, *Mater. Sci. Eng. A.*, 2008, **485**(1-2), p 182-193
6. C.G. Zhou, N. Wang, and H.B. Xu, Comparison of Thermal Cycling Behavior of Plasma-Sprayed Nanostructured and Traditional Thermal Barrier Coatings, *Mater. Sci. Eng. A.*, 2007, **452-453**, p 569-574
7. A. Rauf, Q. Yu, L. Jin, and C. Zhou, Microstructure and Thermal Properties of Nanostructured Lanthana-Doped Yttria-Stabilized Zirconia Thermal Barrier Coatings by Air Plasma Spraying, *Scr. Mater.*, 2012, **66**(2), p 109-112
8. K. Ogawa, D. Minkov, T. Shoji, M. Sato, and H. Hashimoto, NDE of Degradation of Thermal Barrier Coating by Means of Impedance Spectroscopy, *NDT & E Int.*, 1999, **32**, p 177-185
9. X. Wang, J.F. Mei, and P. Xiao, Determining Oxide Growth in Thermal Barrier Coatings (TBCs) Non-Destructively Using Impedance Spectroscopy, *J. Mater. Sci. Lett.*, 2001, **20**, p 47-49
10. P. Anderson, X. Wang, and P. Xiao, Effect of Isothermal Heat Treatment on Plasma-Sprayed Yttria-Stabilized Zirconia Studied by Impedance Spectroscopy, *J. Am. Ceram. Soc.*, 2005, **88**(2), p 324-330
11. F. Yang and P. Xiao, Nondestructive Evaluation of Thermal Barrier Coatings Using Impedance Spectroscopy, *Int. J. Appl. Ceram. Technol.*, 2009, **6**, p 381-399
12. B. Jayaraj, S. Vishweswaraiah, V.H. Desai, and Y.H. Sohn, Electrochemical Impedance Spectroscopy of Thermal Barrier Coatings as a Function of Isothermal and Cyclic Thermal Exposure, *Surf. Coat. Technol.*, 2004, **117-178**, p 140-151
13. J.W. Byeon, B. Jayaraj, S. Vishweswaraiah, S. Rhee, V.H. Desai, and Y.H. Sohn, Non-Destructive Evaluation of Degradation in Multi-Layered Thermal Barrier Coatings by Electrochemical Impedance Spectroscopy, *Mater. Sci. Eng. A.*, 2005, **407**(1-2), p 213-225
14. B. Jayaraj, V.H. Desai, C.K. Lee, and Y.H. Sohn, Electrochemical Impedance Spectroscopy of Porous ZrO_2-8 wt.% Y_2O_3 and Thermally Grown Oxide on Nickel Aluminide, *Mater. Sci. Eng. A.*, 2004, **372**(1-2), p 278-286
15. A. Selcuk and A. Atkinson, The Evolution of Residual Stress in the Thermally Grown Oxide on Pt Diffusion Bond Coats in TBCs, *Acta Mater.*, 2003, **51**(2), p 535-549
16. J.A. Nychka, D.R. Clark, and S. Sridharan, NDE Assessment of TBCs: An Interim Report of a Photo-Stimulated Luminescence 'Round-Robin' Test, *Surf. Coat. Technol.*, 2003, **163-164**, p 87-94
17. X.Q. Ma and M. Takemoto, Quantitative Acoustic Emission Analysis of Plasma Sprayed Thermal Barrier Coatings Subjected

to Thermal Shock Tests, *Mater. Sci. Eng. A.*, 2001, **308**(1-2), p 101-110
18. A. Kucuk, C.C. Berndt, U. Senturk, and R.S. Lima, Influence of Plasma Spray Parameters on Mechanical Properties of Yttria Stabilized Zirconia Coatings. II: Acoustic Emission Response, *Mater. Sci. Eng. A.*, 2000, **284**(1-2), p 41-50
19. A. Lashtabeg, J. Drennan, R. Knibbe, J.L. Bradley, and G.Q. Lu, Synthesis and Characterization of Macroporous Yttria Stabilised Zirconia (YSZ) Using Polystyrene Spheres as Templates, *Microporous Mesoporous Mater.*, 2009, **117**, p 395-401
20. J.S. Cronin, J.R. Wilson, and S.A. Barnett, Impact of Pore Microstructure Evolution on Polarization Resistance of Ni-Yttria-Stabilized Zirconia Fuel Cell Anodes, *J. Power Sources*, 2011, **196**(5), p 2640-2643
21. N.H. Perry and T.O. Mason, Grain Core and Grain Boundary Electrical/Dielectric Properties of Yttria-Doped Tetragonal Zirconia Polycrystal (TZP) Nanoceramics, *Solid State Ionics*, 2010, **181**(5-7), p 276-284
22. N. Wang, C.G. Zhou, S.K. Gong, and H.B. Xu, Heat Treatment of Nanostrutured Thermal Barrier Coating, *Ceram. Int.*, 2007, **33**(6), p 1075-1081
23. Z.L. Wu, L.Y. Ni, Q.H. Yu, and C.G. Zhou, Effect of Thermal Exposure on Mechanical Properties of a Plasma-Sprayed Nanostructured Thermal Barrier Coating, *J. Therm. Spray. Technol.*, 2012, **21**, p 169-175
24. S.H. Song and P. Xiao, An Impedance Spectroscopy Study of High-Temperature Oxidation of Thermal Barrier Coatings, *Mater. Sci. Eng. B.*, 2003, **97**(1), p 46-53
25. J.R. MacDonald, Impedance Spectroscopy, *Ann. Biomed. Eng.*, 1992, **20**, p 289-305
26. T. Hilpert and E. Ivers-Tiffée, Correlation of Electrical and Mechanical Properties of Zirconia Based Thermal Barrier Coatings, *Solid State Ionics*, 2004, **175**(1-4), p 471-476
27. S.T. Amaral and I.L. Muller, Effect of Silicate on Passive Films Anodically Formed on Iron in Alkaline Solution as Studied by Electrochemical Impedance Spectroscopy, *Corrosion*, 1999, **55**, p 17-23
28. I.R. Gibson, G.P. Dransfield, and J.T.S. Irvine, Sinterability of Commercial 8 mol% Yttria-Stabilized Zirconia Powders and the Effect of Sintered Density on the Ionic Conductivity, *J. Mater. Sci.*, 1998, **33**, p 4297-4305
29. X.J. Chen, K.A. Khor, S.H. Chan, and L.G. Yu, Influence of Microstructure on the Ionic Conductivity of Yttria-Stabilized Zirconia Electrolyte, *Mater. Sci. Eng. A.*, 2002, **335**(1-2), p 246-252
30. D. Pérez-Coll, E. Sánchez-López, and G.C. Mather, Influence of Porosity on the Bulk and Grain-Boundary Electrical Properties of Gd-Doped Ceria, *Solid State Ionics*, 2010, **181**(21-22), p 1033-1042
31. M.C. Steil, F. Thevenot, and M. Kleitz, Densification of Yttria-Stabilized Zirconia, *J. Electrochem. Soc.*, 1997, **144**(1), p 390-398